AFRL-SR-BL-TR-99-

0168

38

REPORT DOCUMENTATION PAGE

1. AGENCY USE ONLY (Leave blank)	2. REPORT DATE	3. REPORT TYPE AND DATES COVERED
	9/3/98	Final Technical (03/01/97-02/28/98)

4. TITLE AND SUBTITLE
(FY97 - DURIP)Dynamically Altered Compliant Surface and Measuring Equipment for Use in the Control of Separation by Oscillatory Mean

5. FUNDING NUMBERS
F49620-97-1-0143

6. AUTHOR(S)
Israel Wygnanski, Professor

7. PERFORMING ORGANIZATION NAME(S) AND ADDRESS(ES)
Department of Aerospace and Mechanical Engineering
The College of Engineering and Mines
The University of Arizona
Tucson, AZ 85721

8. PERFORMING ORGANIZATION REPORT NUMBER

9. SPONSORING / MONITORING AGENCY NAME(S) AND ADDRESS(ES)
AFOSR/NA
110 Duncan Avenue, Room B115
Bolling AFB, DC 20332-8050

10. SPONSORING / MONITORING AGENCY REPORT NUMBER

11. SUPPLEMENTARY NOTES

12a. DISTRIBUTION / AVAILABILITY STATEMENT

Approved for Public Release
Distribution is Unlimited

12b. DISTRIBUTION CODE

13. ABSTRACT (Maximum 200 words)

We have selected a vendor (DANTEC) and purchased a three dimensional LDA. The selection process took over 6 months to complete with three companies competing (DANTEC, AEROMETRICS & TSI). The instrument has been installed and was immediately used on two DOD sponsored projects:

1 On a boundary layer that is continuously maintained on the verge of separation (the Stratford ramp), a project that is sponsored by ONR.

2 On studying the separation of a wall jet that flows over a circular cylinder.

In both experiments regions of local, time dependent reverse flow were detected and the typical hot wire was incapable to provide accurate results.

I am enclosing a copy of an article that was very recently accepted for publication by the Journal of Fluid Mechanics after we have checked the reliability of the data with the new equipment that was purchased on this grant (see specifically figures 3-5).

14. SUBJECT TERMS

15. NUMBER OF PAGES
19

16. PRICE CODE

17. SECURITY CLASSIFICATION OF REPORT	18. SECURITY CLASSIFICATION OF THIS PAGE	19. SECURITY CLASSIFICATION OF ABSTRACT	20. LIMITATION OF ABSTRACT
UNCLASSIFIED	UNCLASSIFIED	UNCLASSIFIED	UNLIMITED

DYNAMICALLY ALTERED COMPLIANT SURFACE AND MEASURING EQUIPMENT FOR USE IN THE CONTROL OF SEPARATION BY OSCILLATORY MEANS.

I.WYGNANSKI
Aerospace and Mechanical Engineering Department
The University of Arizona
Tucson AZ. 85721

FINAL REPORT
AFOSR Grant Number: F49620-97-0143

We have selected a vendor (DANTEC) and purchased a three dimensional LDA. The selection process took over 6 months to complete with three companies competing (DANTEC, AEROMETRICS & TSI). The instrument has been installed and was immediately used on two DOD sponsored projects:

1 On a boundary layer that is continuously maintained on the verge of separation (the Stratford ramp), a project that is sponsored by ONR.

2 On studying the separation of a wall jet that flows over a circular cylinder.

In both experiments regions of local, time dependent reverse flow were detected and the typical hot wire was incapable to provide accurate results.

I am enclosing a copy of an article that was very recently accepted for publication by the Journal of Fluid Mechanics after we have checked the reliability of the data with the new equipment that was purchased on this grant (see specifically figures 3-5).

On a Turbulent Wall Jet Flowing Over a Circular Cylinder

by

R. Neuendorf and I. Wygnanski

AME Department

University of Arizona

Tucson, AZ 85721

submitted in April, 1997
&
in revised form in June, 1998

Abstract

The effect of surface curvature on the development of a two-dimensional wall jet was investigated experimentally. A comparison was made between a wall jet flowing around a circular cylinder and its plane equivalent. Velocity surveys and surface pressure measurements in the curved wall jet suggest the existence of two primary regions of interest. The first region, ranging from the end of the potential core to an approximate angular position of $\theta = 120°$, is characterized by a constant surface pressure and a self similarity of the mean flow. The second region is marked by an adverse pressure gradient leading to separation around $\theta = 230°$. The rate of spread of this flow, even in the initial region, is much higher than in the plane wall jet and so are the levels of turbulence and Reynolds stress. The dominant length scale in this flow is the radius of curvature R and the dominant velocity scale is the square root of the kinematic jet momentum divided by the radius of curvature. Entrainment of ambient fluid which causes the jet to adhere to the curved surface is also the main reason for its separation which is preceded by a rapid rate of spread of the flow leading to the failure of the boundary layer approximation.

and Fekete provides such an opportunity. The present data is compared to measurements made on a plane wall jet by Zhou, Heine and Wygnanski (1996).

The tests were carried out on a smooth, circular cylinder at slot Reynolds numbers ranging from $3 \cdot 10^3$ to $13 \cdot 10^3$. Taps drilled through the cylinder walls were used to provide mean surface pressure data, while velocity measurements were carried out using hot-wire anemometers.

2. Apparatus and Data Acquisition

The experiments were carried out on a highly polished, (radius $R = 101.6mm$) circular cylinder on loan from Professors Newman and Fekete of McGill University. The cylinder is made out of a thick aluminum pipe 914.4 mm long that is spliced along its entire length to provide a nozzle as shown in figure 1. The interior space of the cylinder contains the settling chamber, screens, and a contraction through which the jet emerges tangentially to the exterior surface. The width of the nozzle, b, which spans the entire cylinder, can be altered by the addition of spacers at the foot of the upper lip. The initial aspect ratio of the jet varied therefore, between 120 to 350 depending on the spacers used. The cylinder was mounted on bearings embedded inside two large end-plates that allowed rotation around its axis.

The airflow was provided by a centrifugal blower that was powered by a frequency-controlled AC motor. It entered the settling chamber through both ends of the cylinder. Before entering the blower, the air passed through a temperature controlled chamber equipped with cooling coils and a heater that equated the temperature of the jet to the ambient air at all speeds considered. The maximum temperature differential between the two flows did not exceed ±0.5°C.

The hot-wire probe was mounted on a single-axis traverse system in a direction perpendicular to the surface. A computer-controlled stepper motor was used to achieve a resolution of 1/630mm per step. The circumferential distance between the probe and the nozzle was altered by rotating the cylinder. Movements in spanwise direction were accomplished by sliding the traverse on a rail attached to the end-plates and located well above the surface of the cylinder. This freedom of movement was necessary to verify the two-dimensionality of the flow.

The momentum emanating from the nozzle was actually measured by integrating the velocity profile at the slot exit (e.g. figure 2), not relying on the assumption that the flow at the slot has "top hat" velocity profile. The calibration yielded: $0.89 \le 2\rho \int_0^{\infty} \overline{u^2} dy / (p_0 - p_\infty) b \le 0.93$ and the results were normalized by the measured jet momentum. Since the hot wire anemometers were calibrated in a separate calibration jet one could show that the pressure difference between the settling chamber and the room was less than the

Wherever the flow was separated even intermittently (i.e. at $\theta>200°$) the insensitivity of hot wire to directional changes resulted in r_{valid} <90% and it increased the discrepancy between measurements made with a LDA and a hot wire. Intermittent separation affected mostly the measurements of turbulent intensity and not mean velocity as the high turbulence intensity did in the outer part f the wall jet. Because of this uncertainty the results presented and discussed below focus on the region bound by $40°<\theta<200°$. The skin friction estimation was made from the slope of the mean velocity profile in the immediate vicinity of the wall. Great care, therefore, was exercised to measure (dU/dy) as precisely as possible. A comparison between LDA and hot wire data measured in the immediate vicinity of the surface is shown in figures 5a,b for $\theta=60°$ and for 120°. The comparison between the two sets of results is excellent and would result in identical skin friction coefficient. Consequently the various momentum budgets presented below are accurate and reaffirm the two dimensionality of the mean flow.

Measurements done with an LDA (and a PIV for this matter) proved to be sensitive to the source of the seeding particularly at small values of θ. Smoke introduced into the settling chamber biased the mass flow emanating from the nozzle while smoke introduced to the ambient fluid accentuated the entrained flow. Thus the radial velocities measured by tracking the particles could have had an opposite sign depending on their origin.

3. The Mean Velocity profiles

Mean velocity profiles were measured for several jet exit velocities and slot widths, but only a sample of the data is presented for the sake of clarity. All of the data discussed initially corresponds to a single slot width of 2.34 mm and an exit velocity of $U_{jet}=48\frac{m}{sec}$ (see figure 6), and thus a nominal Reynolds number

$$Re_N \equiv \left(\frac{\frac{1}{2}U_{jet}^2 bR}{\nu^2}\right)^{\frac{1}{2}} = 33000$$ (the reason for the choice of this length scale will be apparent later).

A fully developed velocity profile typical to the wall jet flow was observed for this case at an angular position $\theta \approx 20°$. At much larger slot widths the potential core might not have terminated at this location and thus, the first mean velocity profile presented in figure 6 was taken at $\theta=40°$. Since the surface pressure is almost constant up to $\theta=120°$, an attempt was made to plot all the velocity profiles in self-similar coordinates in order to assess the effect of constant curvature on the development of this flow (figure 6). The mean velocity distribution in the curved wall jet is almost indistinguishable from the plane wall jet when it is normalized by the local maximum velocity U_{max} and the distance from the wall y_2 at which the velocity in the outer part of the flow is equal to $\frac{1}{2}U_{max}$. The variation of the local length and velocity scales with distance from nozzle will be examined later. The average location of the maximum velocity occurred at $y/y_2=0.16$, which agrees with the corresponding value for the plane wall jet

linearly with x, or rather with Rθ, as indicated by the solid lines obtained for the plane wall jet at corresponding $Re_j = U_{jet}\, b/\nu$ (figure 9a). The maximum velocities in the curved wall jet decrease much faster with x than in the plane flow. This must be accompanied by an increased rate of spread (figure 9b), otherwise the momentum loss to skin friction would have been unreasonable. It is clear that traditional scaling using the slot width as the reference length scale does not collapse the data onto a single universal curve for different slot widths. Since the mean velocity profiles are self similar, provided $\theta \le 180°$, one may obtain the local, kinematic jet momentum:

$$J = U_{max}^2 y_2 \underbrace{\int_{y/y_2=0}^{\infty} \left(\frac{U}{U_{max}}\right)^2 d\left(\frac{y}{y_2}\right)}_{const} = 0.78 U_{max}^2 y_2 \qquad \text{(eq. 4.1)}$$

from the product of the length and velocity scales. The decay of J in the direction of streaming is very gradual. In the constant surface pressure region $(40° \le \theta \le 120°)$, the skin friction appears to have little or no influence on the evolution of the flow, although the presence of the solid surface affects the scale of the large eddies which are smaller than in a corresponding free jet.

It was recognized by Narasimha (1973) et al. and reinforced by Wygnanski, Katz and Horev that the details of the flow through the nozzle can not influence the overall behavior of the turbulent wall jet far downstream of its origin. Thus the dimension of the nozzle becomes irrelevant. The flow in the absence of curvature scaled with the initial, kinematic momentum flux J and the fluid viscosity ν rather than the slot width b and the exit velocity U_{jet}. The length and velocity scales derived from these two independent parameters are ν^2/J and J/ν respectively. The practical demonstration that the flow is indeed independent of the conditions at the nozzle was provided by Zhou and Wygnanski (1992) who collapsed all the available mean flow data on wall jets onto universal curves independent of $Re_j = U_{jet}\, b/\nu$. It should be noted that the new length and velocity scales based on J and ν define a **Reynolds number which is equal to unity regardless of the conditions at the nozzle.**

The evolution of an incompressible wall jet around the circular cylinder of radius R, depends on J, ν and on R. The significance of the additional length scale R is apparent when the ratio of y_2/R is no longer small. In this instance the boundary layer approximation may no longer apply imposing a new limitation on the slot width (i.e. $b/R \ll 1$). Assuming that the relevant length and velocity scales in the present flow are: R and $(J/R)^{1/2}$ respectively, then the relevant Reynolds number

$$Re_N \equiv \frac{(J/R)^{1/2} R}{\nu} = \frac{(JR)^{1/2}}{\nu} \qquad \text{(eq. 4.2)}$$

instead of being a constant as it was in the plane wall jet. Thus the relevance of the abovementioned Re_N is clearly demonstrated by plotting $\frac{y_2}{\nu^2/J}$ and $\frac{U_{max}}{J/\nu}$ versus the dimensionless distance from the nozzle

This normalization was chosen since to first order of approximation $J_N = \frac{2b}{\rho}(P_0 - P_\infty)$ and P_o is the total pressure in the settling chamber. The integral on the right hand side of the equation represents J and thus under ideal conditions (when $J_N = J$) c_p=2. One may quickly assess the value of c_p in the fully developed, self similar region ($40° \le \theta \le 120°$) by assuming the jet to be thin (i.e. $y/R \to 0$) and neglecting the contribution of the turbulence intensity to the total momentum flux. In this case $c_p = 1.56\, U_{max}^2\, y_2 = 1.92\,(\theta - \theta_o)^{-0.06}$, when the appropriate scaling values are substituted from equation 4.3. The complete right hand side of equation 5.2 is plotted in figure 12. The agreement between this calculation and the measured c_p is reasonable up to θ=160°. At larger azimuthal angles the validity of the boundary layer approximation becomes questionable and higher order terms have to be included.

Newman (1961) derived the scaling parameters for the surface pressure by using dimensional analysis, assuming the flow to be incompressible and governed by:

$$(P_o - P_s),\ b,\ R,\ \rho,\ \nu$$

where ν is the kinematic viscosity of the fluid.

Thus, the surface pressure coefficient c_p, at an angular position θ, is a function of these parameters. Newman realized that at some distance from the nozzle the flow will be independent of the separate parameters $(P_o - P_s)$ and b, but will depend on their product instead [i.e. $(P_0 - P_\infty)b = 2\rho J_N$] leading to:

$$c_p = \frac{(P_\infty - P_s)R}{(P_o - P_\infty)b} = f\left[\theta, \sqrt{\frac{(P_o - P_\infty)Rb}{\rho\nu^2}}\right] \qquad \text{(eq. 5.3)}$$

where Newman's Reynolds number $Re_N = \sqrt{\frac{(P_o - P_\infty)Rb}{\rho\nu^2}}$ contains the product of the two length scales. The same quantity appeared in conjunction with the scaling of the mean velocity distribution in this flow (see eq. 4.2). For large values of this Reynolds number, c_p should also become independent of Re_N as it did in the case of the mean velocity. Thus the surface pressure becomes merely a function of θ. It remains to be seen whether the independent ratio b/R, which was thus far neglected, is of any significance. In order to answer this question, the slot width b and the initial jet velocity U_{jet} were varied in a manner that maintained constant Reynolds numbers (Re_N 19000, Re_N 33000 and Re_N 51000) for different ratios b/R. The symbols representing the nine independent experiments are listed below:

present study[1]. The scatter apparent in figure 12 can be reduced by recalling that J_N is only an approximation to the jet momentum, because the flow expands from the settling chamber to the local static pressure prevailing near the nozzle, P_s. Thus if $J = \frac{2b}{\rho}(P_0 - P_s)$ then the modified pressure coefficient

$$[c_p]_M = \frac{(P_\infty - P_s)R}{1/2\rho J} = \frac{(P_\infty - P_s)R}{J_N(1 + c_p\frac{b}{R})} = \frac{c_p}{(1 + c_p\frac{b}{R})} \qquad \text{(eq. 5.4)}$$

reduces the scatter but does not eliminate it entirely.

6. Skin Friction and Mean Momentum Balance

The skin friction coefficient was determined from the slope of the mean velocity profile close to the surface. This measuring technique was adopted earlier for the plane wall jet, it is based on 6-10 data points taken in the region where the velocity gradient is linear. In the present case, it allowed a reexamination of the character of the velocity distribution prior to separation. Specifically it was searched for the occurrence of inflection points in the adverse pressure gradient region seen prior to the mean separation location. When the skin friction is normalized by the local maximum velocity $\tau_w/\rho U_{max}^2$, it appears to increase with increasing θ attaining a maximum value around $\theta = 140°$ (figure 13b). This peculiar behavior stems from changes in U_{max} rather then in τ_w. Using J_N/R for normalization indicates that c_f decreases monotonically with increasing distance from the nozzle (figure 13c). The centrifugal forces associated with the convex curvature reduce c_f. The c_f measured presently is 1/3 of the corresponding c_f measured in the plane wall jet configuration (figure 13d).

One may now assess the consistency of the measurements, the validity of the boundary layer approximation and the two-dimensionality of the flow by constructing a control volume around the cylinder and checking the mean momentum balance. Starting at $\theta = 40°$ where similarity of the mean flow was observed and considering the constant pressure region first (i.e. going around a 1/4 of the circle up to $\theta = 130°$) yields the following balance in the vertical direction (see figure 14):

$$\left[\int_0^{\bar{}} (c_p J/2R) - U^2)dy\right]_{\theta=130°} + J/2\int_0^{\pi/2}(c_p \cos\theta + \frac{R}{b}c_f \sin\theta)d\theta = 0 \qquad \text{(eq. 6.1)}$$

the sum of all four terms computed from the data amounts to (0.036J) proving the overall consistency of the measurements and the two dimensionality of the flow. The contribution of the skin friction to this balance is minimal 0.015 J and therefore this momentum budget can not be used as a proof of reliability of this data. One may repeat this exercise between $\theta = 40°$ and 220° by assuming that the jet enters and leaves the control volume in the horizontal direction giving:

[1] Surface visualization was used initially, more recently however, the fluid emerging from the slot was seeded with smoke particles and a 2D laser sheet illumination was used. No bubble was observed near the slot.

surface then at $\theta \leq 160°$ (one should recall that u′ is plotted vs. y/y_2 and that y_2 increases rapidly with θ when $\theta \geq 180°$). There is a correlation between the production of turbulent energy near the surface $\left(\overline{u'v'}\frac{\partial U}{\partial y}\right)$ and the maximum intensity of u' observed. Some of it is masked by normalizing the turbulence by local U_{max} (see also figure 13c,d); however, plotting $\left(\frac{\overline{u'^2}}{J/R}\right)^{1/2}$ does not alter the distribution of $\sqrt{\overline{u'^2}}$ with y/y_2. The distribution of $\sqrt{\overline{u'^2}}/U_{max}$ with y/y_2 is plotted on an expanded scale in figure 17b. The radial component of the velocity fluctuations $\sqrt{\overline{v'^2}}/U_{max}$ is initially comparable with its counterpart on the flat plate but its magnitude doubles between $40° \leq \theta \leq 200°$ (figure 17c). The radial location at which the local value of $\sqrt{\overline{v'^2}}/U_{max}$ is maximum decreases with respect to y_2 with increasing θ. Therefore at $\theta = 40°$ $y_{(v'=max)}/y_2 = 0.7$ while at $\theta = 200°$ $y_{(v'=max)}/y_2 = 0.35$. One might have expected that the y-location at which u′v′ attains its maximum will also decrease relative to y_2, at large values of θ, however, this was not the case as may be noted in figure 17e. Between $\theta = 40°$ and $\theta = 200°$: $\left[\sqrt{\overline{u'^2}}/U_{max}\right]_{max}$ increased by a factor of 1.65, $\left[\sqrt{\overline{v'^2}}/U_{max}\right]_{max}$ increased by a factor of 2 and $\left[\overline{u'v'}/U^2_{max}\right]_{max}$ by a factor of 2.4; however, $U_{max.}$ decreased by a factor of 4 in this $\Delta\theta$ interval. The ratio between $(u'/v')_{max}$ decreased from 1.4 at $\theta = 40°$ to 1.08 at $\theta = 160°$. The maximum of the $\overline{u'v'}$ correlation (figure 18) exceeds 0.53 which is larger than in the plane wall jet on (where $\frac{\overline{u'v'}}{\sqrt{\overline{u'^2}}\sqrt{\overline{v'^2}}} = 0.49$) and significantly larger than in the turbulent boundary layer over a flat plate. The radial location at which $\frac{\overline{u'v'}}{\sqrt{\overline{u'^2}}\sqrt{\overline{v'^2}}}$ attains its maximum value increases with θ from being at $y/y_2 = 0.5$ at $\theta = 40°$ to $y/y_2 = 1$ at $\theta = 160°$. Since these observations are peculiar to this flow they suggest that surface curvature and the centrifugal force generated by it, alter the turbulent structure.

The Reynolds stress was calculated from the momentum equation in the direction of streaming (eq. 7.1) which included the pressure gradient term obtained from the normal momentum equation (eq. 7.2) but neglected the viscous term.

comparable to the tangential one, the flow separates. The present measurements indicate that the boundary layer approximation, used to describe turbulent jets of all kinds, fails (*a long time*) before the onset of separation. This suggests that entrainment acts like a double edged sword, a threshold value is required to get a jet to adhere to a surface but it should be kept to a minimum in order to prevent or delay its separation from the surface.

9. References

Bradshaw, P "Effects of Streamline Curvature on Turbulent Flow", AGARDograph No. 169

Fekete, G.I. "Coanda Flow of a two-dimensional wall jet on the outside of a cylinder", McGill University (Montreal Quebec, Canada), August 1963

Fujisawa, N. Kobayashi "Turbulence Characteristics of Wall Jets Along Strong Convex Surfaces", Jour. Mech. Sci. Vol. 29, No.5, 1987

Goldstein 1938, "Modern Development in Fluid Dynamics", Vol. 1

Guitton, D.E. 1964 "Two-dimensional turbulent wall jets over curved surfaces", Mech. Eng. Res. Lab. Report 64-7, McGill University or NASA Technical Reports 19640012572 N (64N22486)

Launder, B.E., Rodi, W. 1981, "The Turbulent Wall Jet", Prog. Aerospace Sci. 19, 81

Meroney, R.N. 1973, unpublished work, Imperial College, quoted by Bradshaw

Nakaguchi, H. 1961, "Jet Along a Curved Wall" Research Memo. No. 4, Dept. of Aeronautics, Univ. Tokyo

Narasimha, R., Narayan, K.Y. and Parthasarathy, S.P. 1973, "Parametric Analysis of Turbulent Wall Jets in Still Air", Aerospace Journal 77, p. 355

Newman, B.G. 1961, "The Deflection of Plane Jets by Adjacent Boundaries - Coanda Effect" in Boundary Layer and Flow Control, G.V. Lachman (ed), Pergamon Press

Newman, B.G. 1969, "The Prediction of Turbulent Jets And Wall Jet", Can. Aerospace Jour. Vol. 15, No. 8

Rayleigh 1916, "On the Dynamics of Revolving Fluids", Proc. Roy. Soc., A, Vol. XCIII, p. 148

Townsend, A.A. 1961, "The Behavior of a Turbulent Boundary Layer Near Separation", JFM Vol. 12

Wilson, D.J., 1976 Goldstein, R.J. "Turbulent Wall Jet With Cylindrical Streamwise Surface Curvature", JFE September 1976

Wygnanski, Katz and Horev 1992, "On The Applicability of Various Scaling Laws to The Turbulent Wall Jet", JFM Vol. 234

Young, T. 1800, "Outlines of Experiments and Inquiries Respecting Sound and Light", Lecture to the Royal Society Jan 16 1800 (see. Jour. Roy. Aero. Soc., Vol. 61, 1957, p.157)

Zhou, M.D. 1992, "On The Hydrodynamic Stability of The Wall Jet", 11th Austr. Fl. Mech. Conference

Zhou, M.D., Heine, Chr., Wygnanski, I. 1996, "The effect of excitation on the coherent and random motion in a plane wall jet", JFM vol. 310

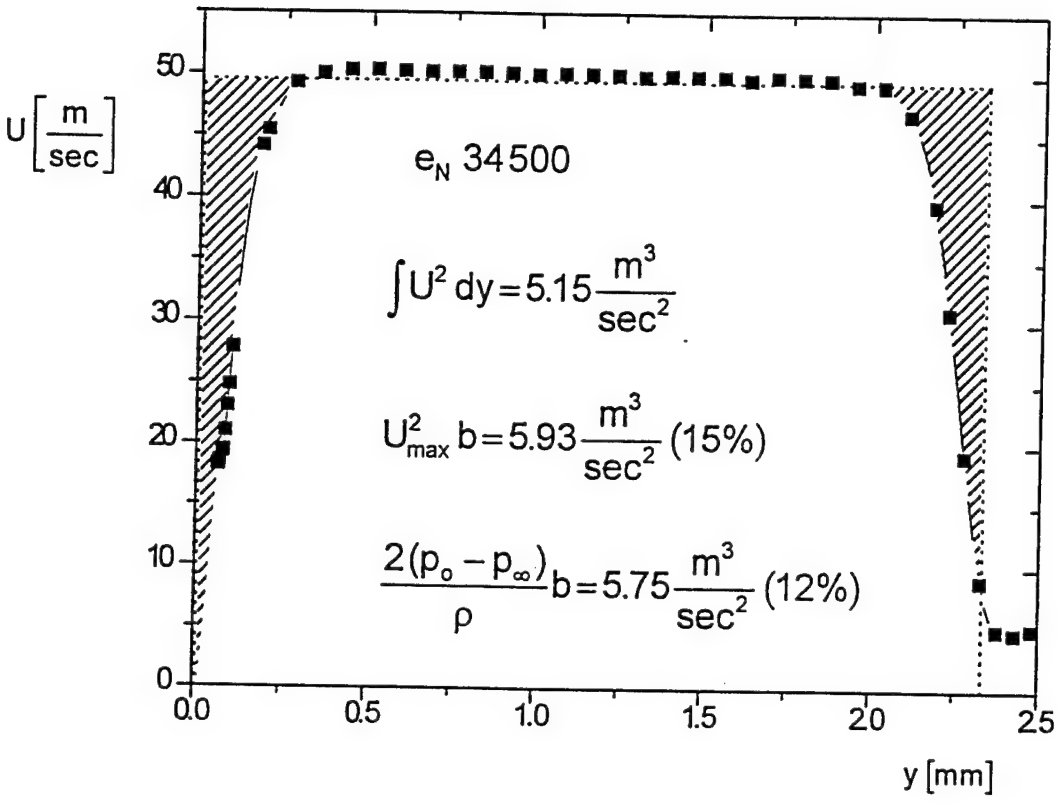
U [m/sec]
50
40
30
20
10
0
0.0
0.5
1.0
1.5
2.0
2.5
y [mm]
e_N 34500
$\int U^2 dy = 5.15 \frac{m^3}{sec^2}$
$U^2_{max} b = 5.93 \frac{m^3}{sec^2}$ (15%)
$\frac{2(p_o - p_\infty)}{\rho} b = 5.75 \frac{m^3}{sec^2}$ (12%)

figure 2

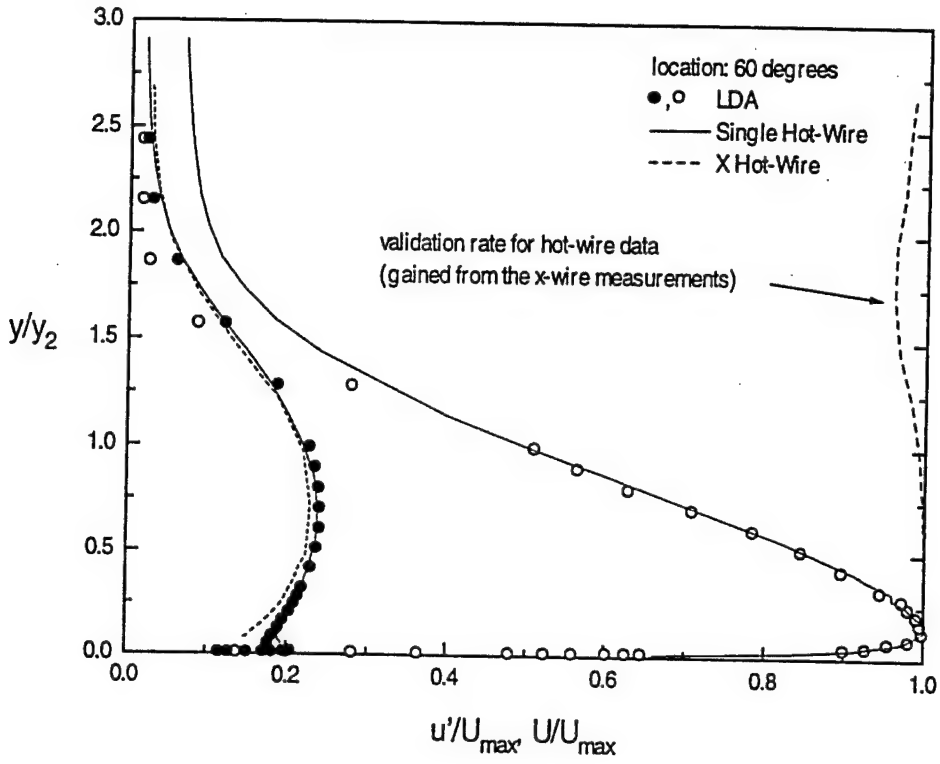

figure 4a

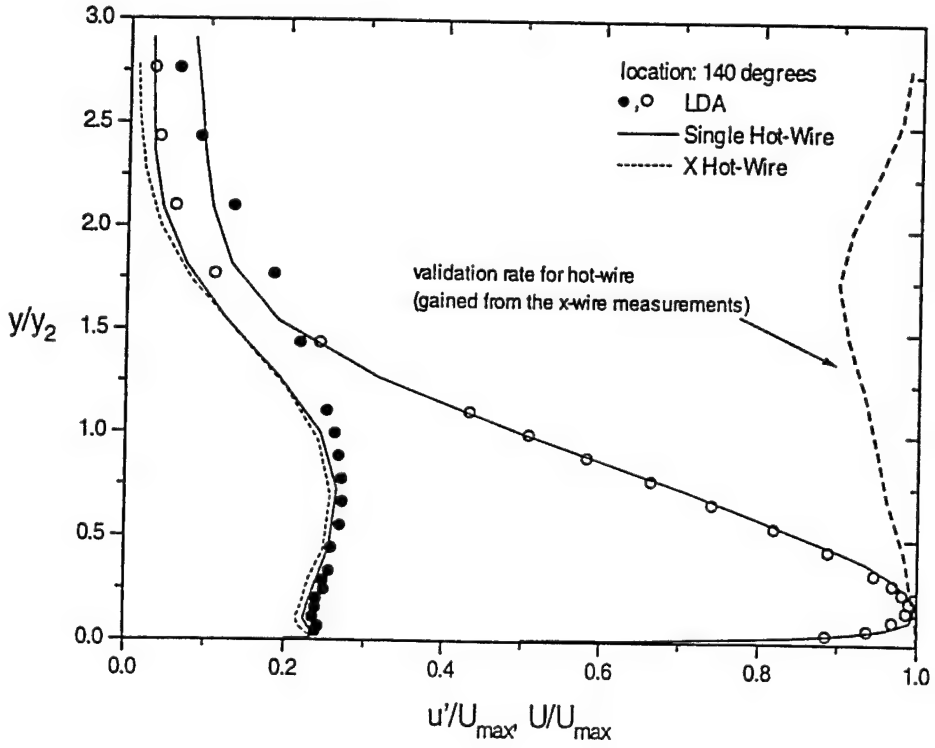

figure 4b

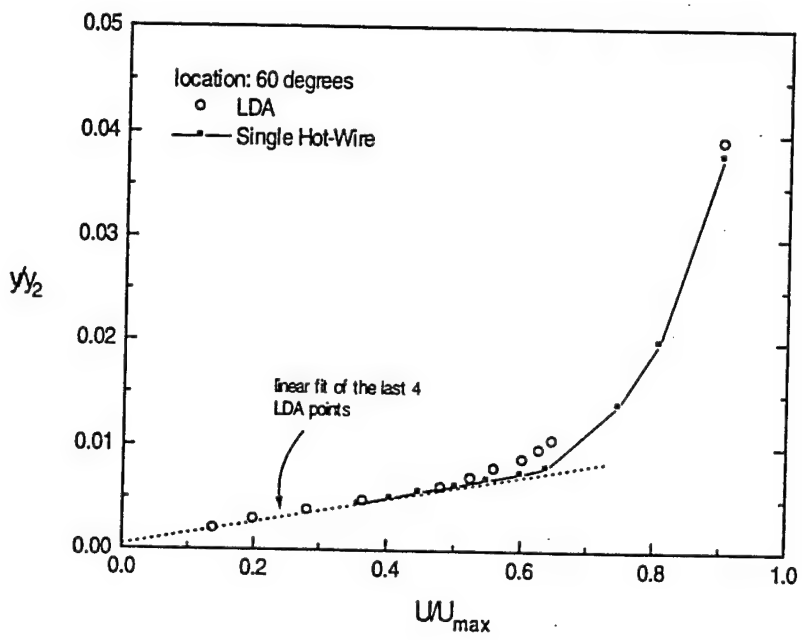

figure 5a

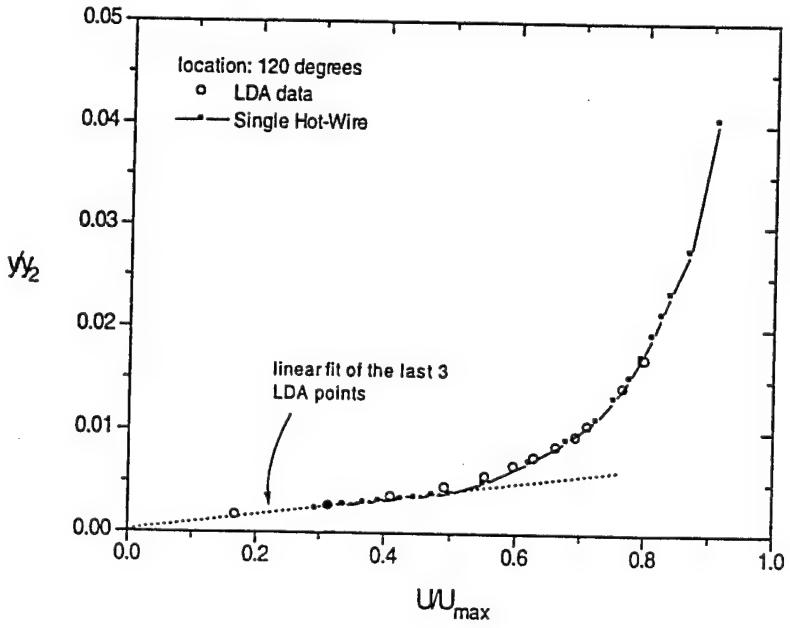

figure 5b

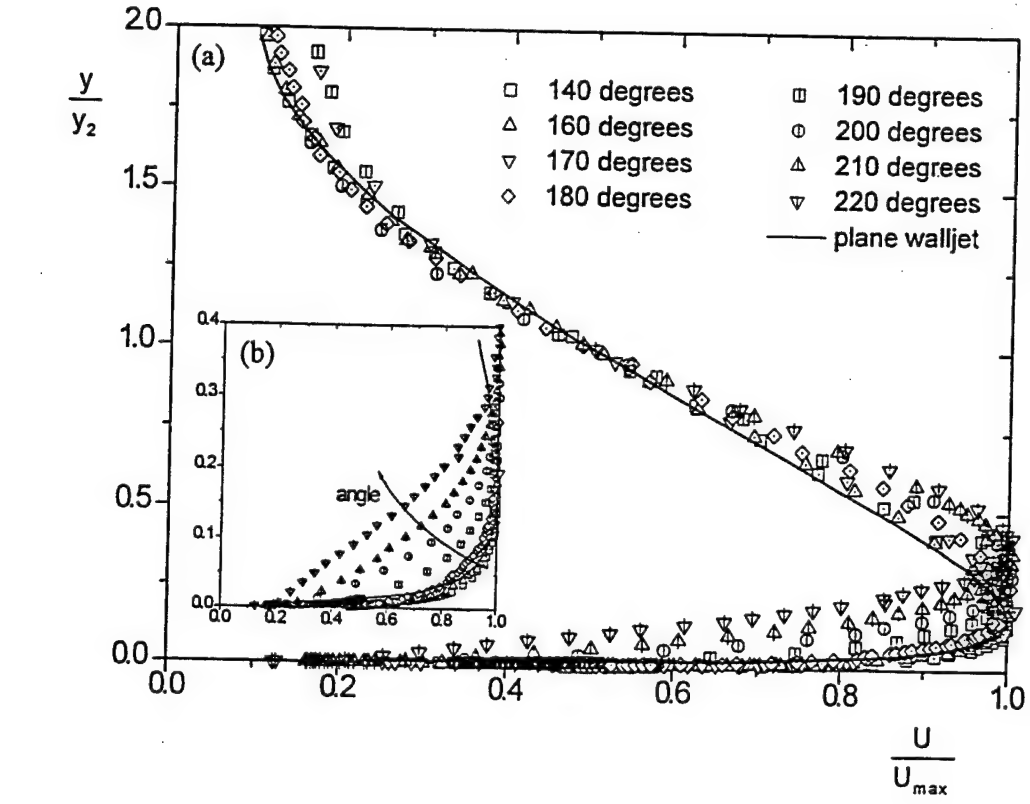
(a)
y / y2
140 degrees
160 degrees
170 degrees
180 degrees
190 degrees
200 degrees
210 degrees
220 degrees
plane walljet
(b)
angle
U / Umax

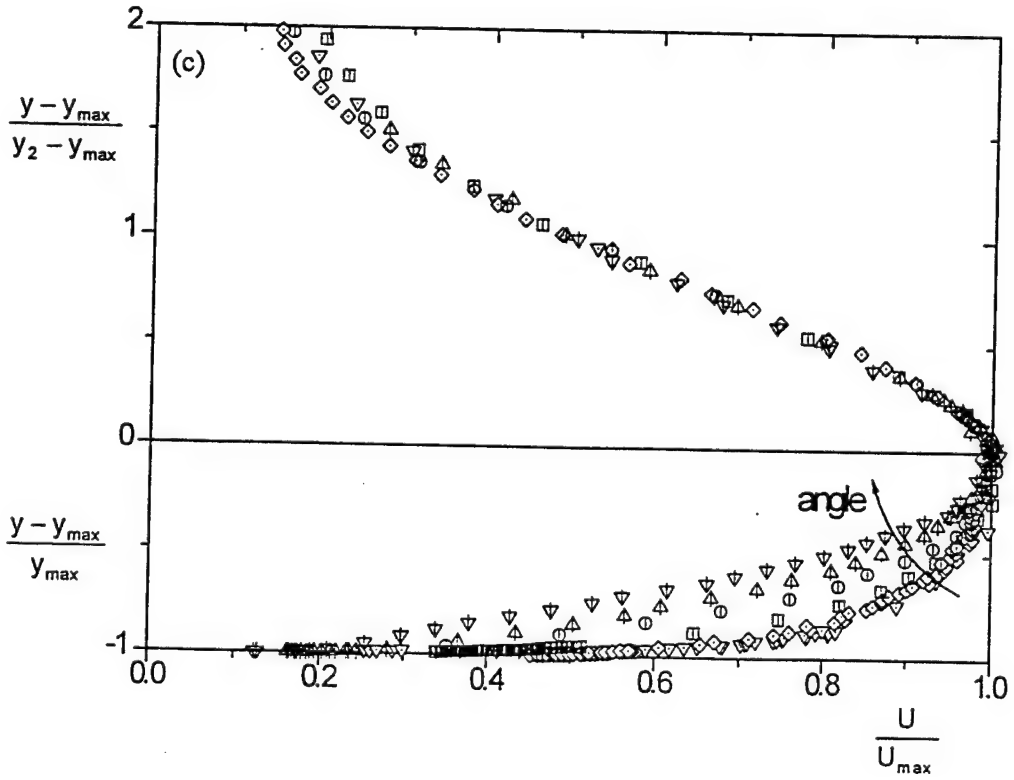
(c)
(y − ymax) / (y2 − ymax)
(y − ymax) / ymax
angle
U / Umax

figure 7

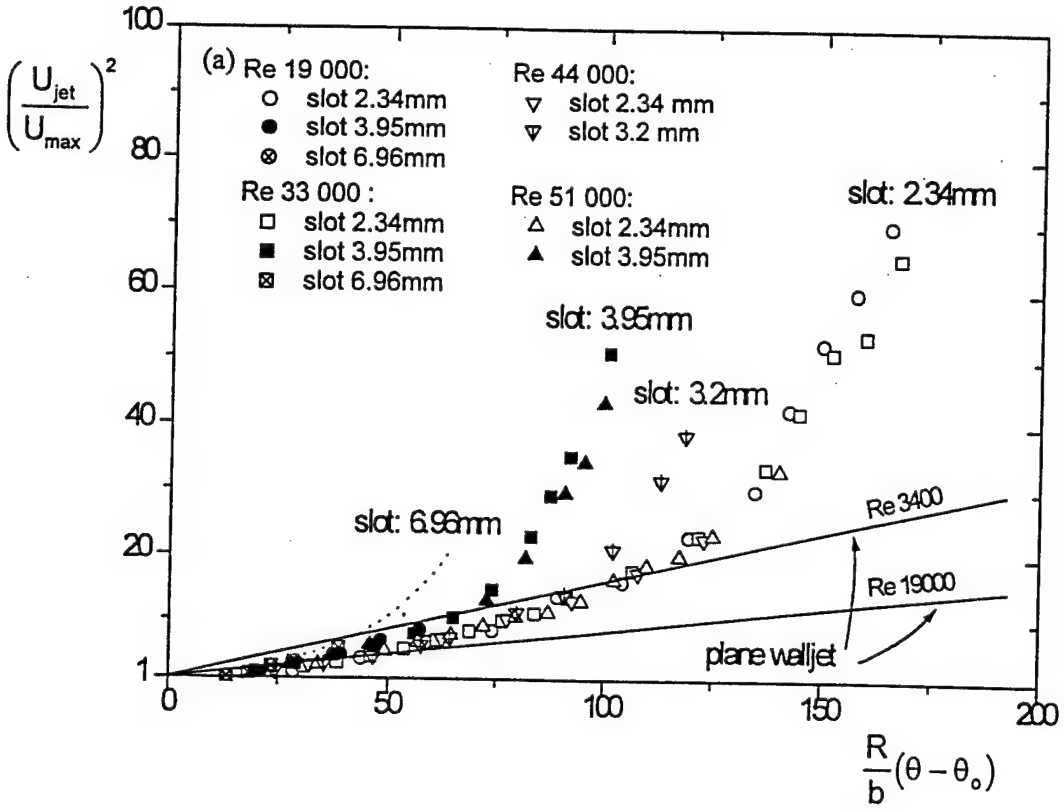
(a)
$\left(\frac{U_{jet}}{U_{max}}\right)^2$
Re 19 000:
slot 2.34mm
slot 3.95mm
slot 6.96mm
Re 33 000 :
slot 2.34mm
slot 3.95mm
slot 6.96mm
Re 44 000:
slot 2.34 mm
slot 3.2 mm
Re 51 000:
slot 2.34mm
slot 3.95mm
slot: 2.34mm
slot: 3.95mm
slot: 3.2mm
slot: 6.96mm
Re 3400
Re 19000
plane walljet
100
80
60
40
20
1
0
50
100
150
200
$\frac{R}{b}(\theta-\theta_o)$

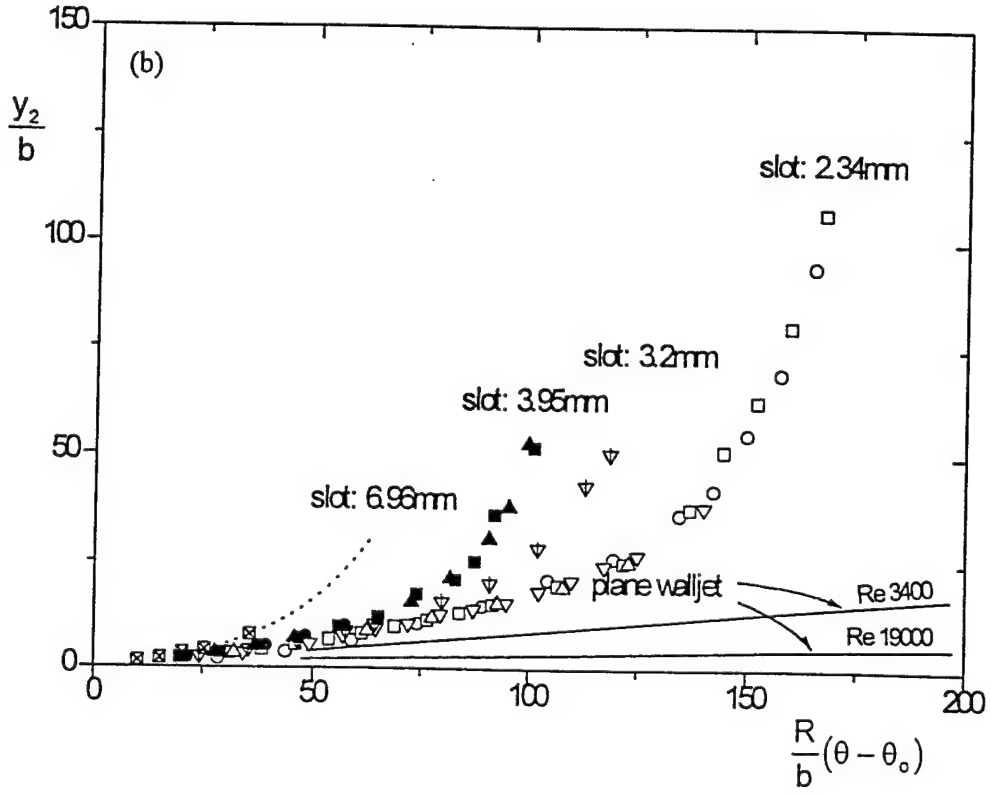
(b)
$\frac{y_2}{b}$
slot: 2.34mm
slot: 3.2mm
slot: 3.95mm
slot: 6.96mm
plane walljet
Re 3400
Re 19000
150
100
50
0
0
50
100
150
200
$\frac{R}{b}(\theta-\theta_o)$

figure 9

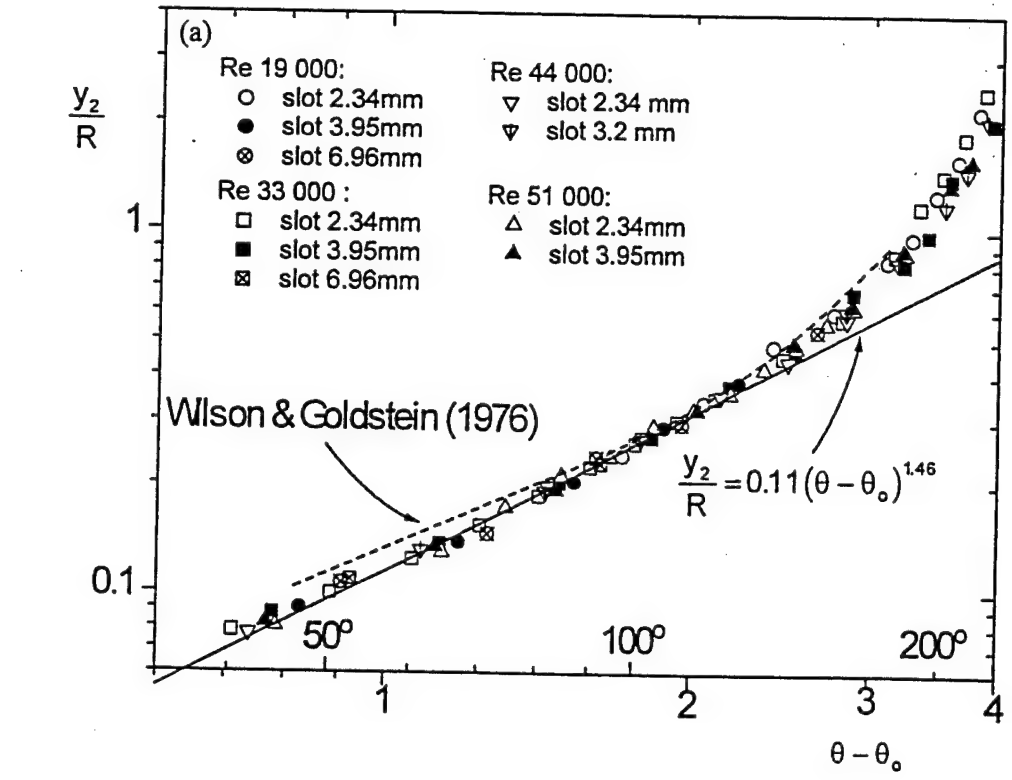
(a)
Re 19 000:
slot 2.34mm
slot 3.95mm
slot 6.96mm
Re 33 000 :
slot 2.34mm
slot 3.95mm
slot 6.96mm
Re 44 000:
slot 2.34 mm
slot 3.2 mm
Re 51 000:
slot 2.34mm
slot 3.95mm
$\frac{y_2}{R}$
1
0.1
Wilson & Goldstein (1976)
$\frac{y_2}{R} = 0.11(\theta - \theta_o)^{1.46}$
50°
100°
200°
1
2
3
4
$\theta - \theta_o$

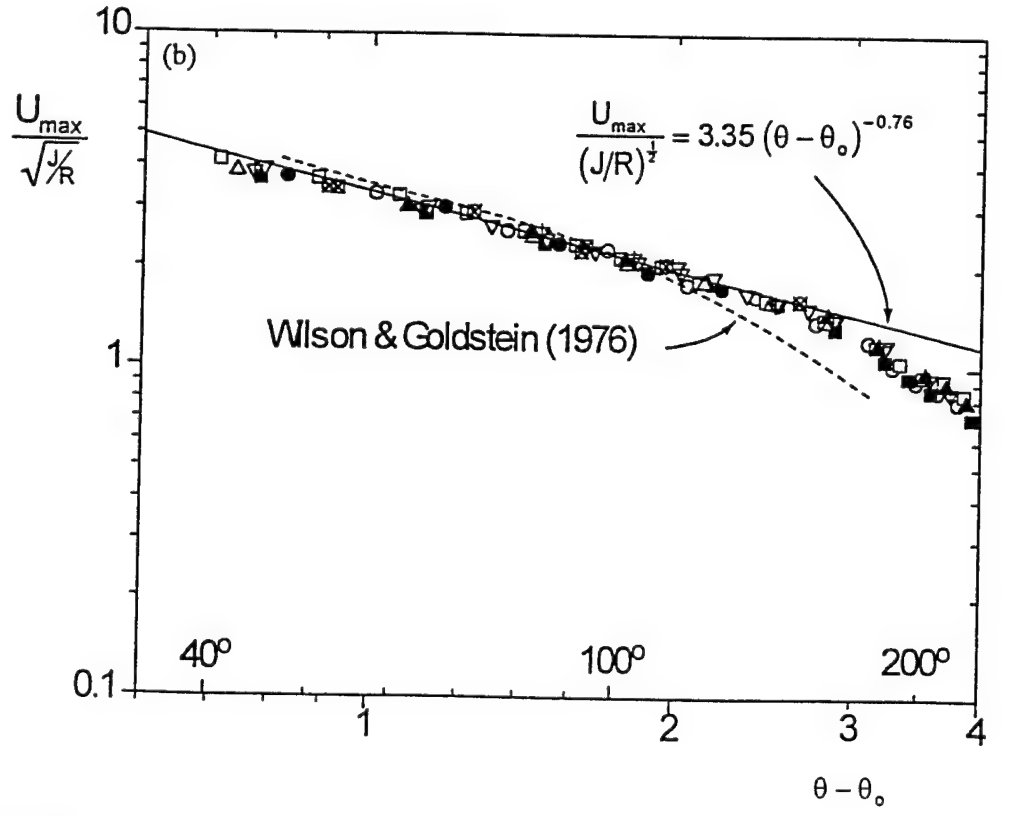
10
(b)
$\frac{U_{max}}{\sqrt{J/R}}$
$\frac{U_{max}}{(J/R)^{\frac{1}{2}}} = 3.35(\theta - \theta_o)^{-0.76}$
Wilson & Goldstein (1976)
1
0.1
40°
100°
200°
1
2
3
4
$\theta - \theta_o$

figure 11

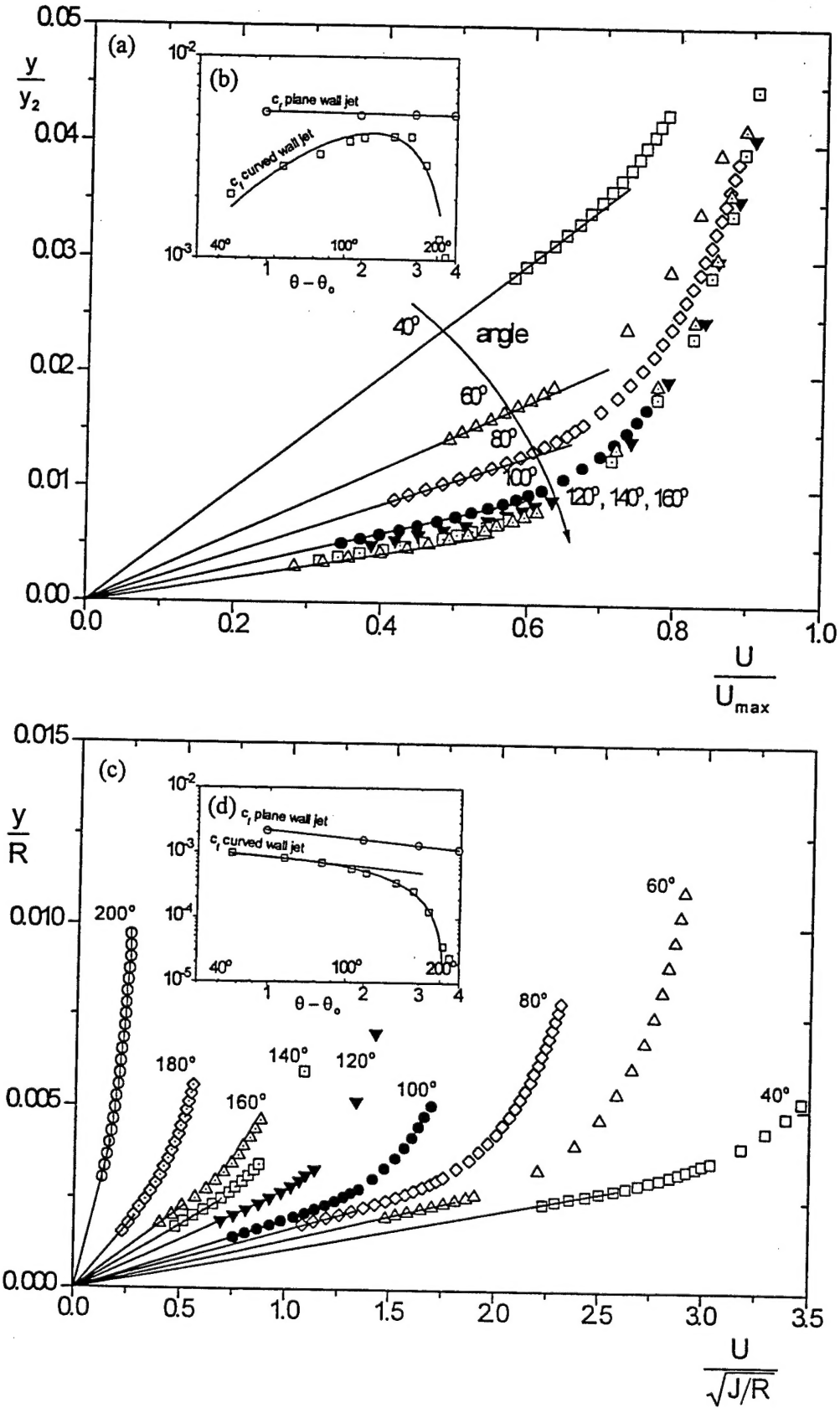
(a)
(b)
(c)
(d)
y/y2
y/R
U/Umax
U/√(J/R)
angle
40°
60°
80°
100°
120°, 140°, 160°
200°
180°
160°
140°
120°
100°
80°
60°
40°
c_f plane wall jet
c_f curved wall jet
θ − θ_o

figure 13

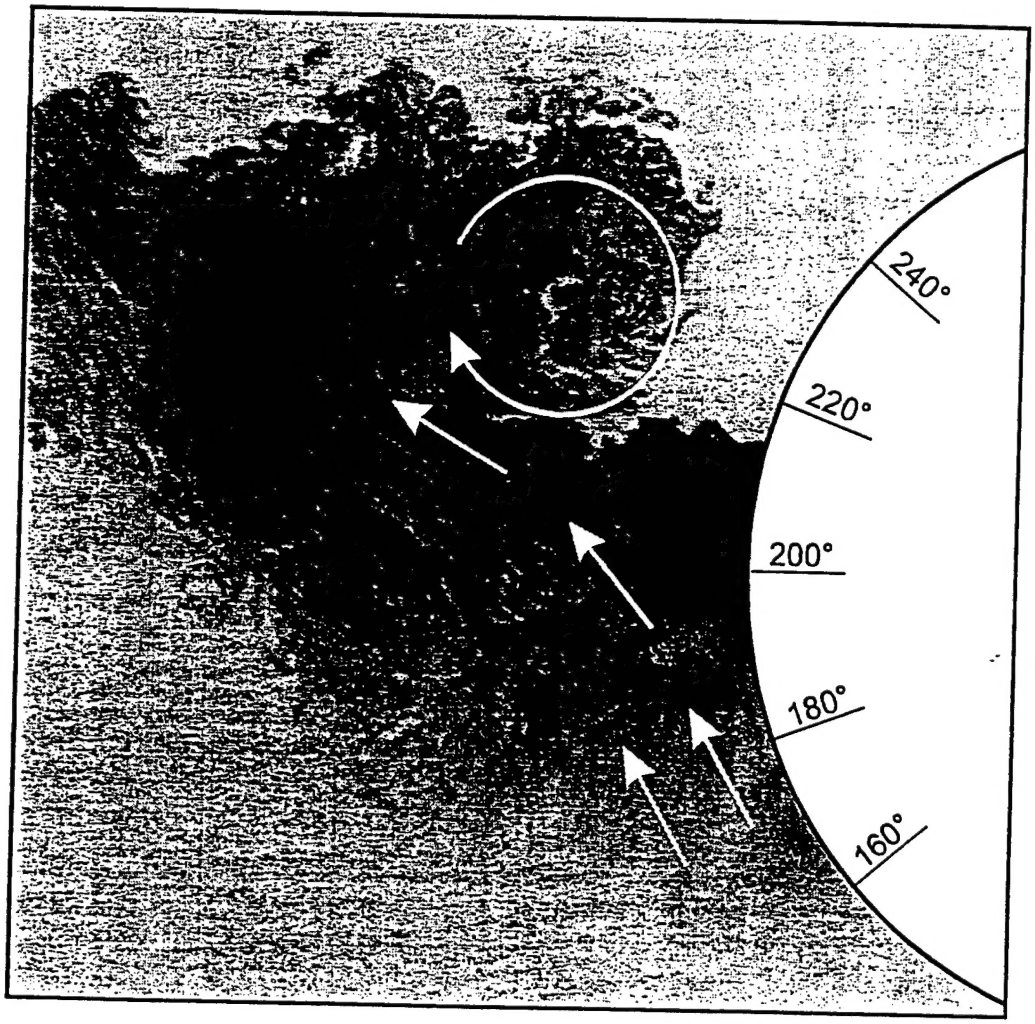

figure 15

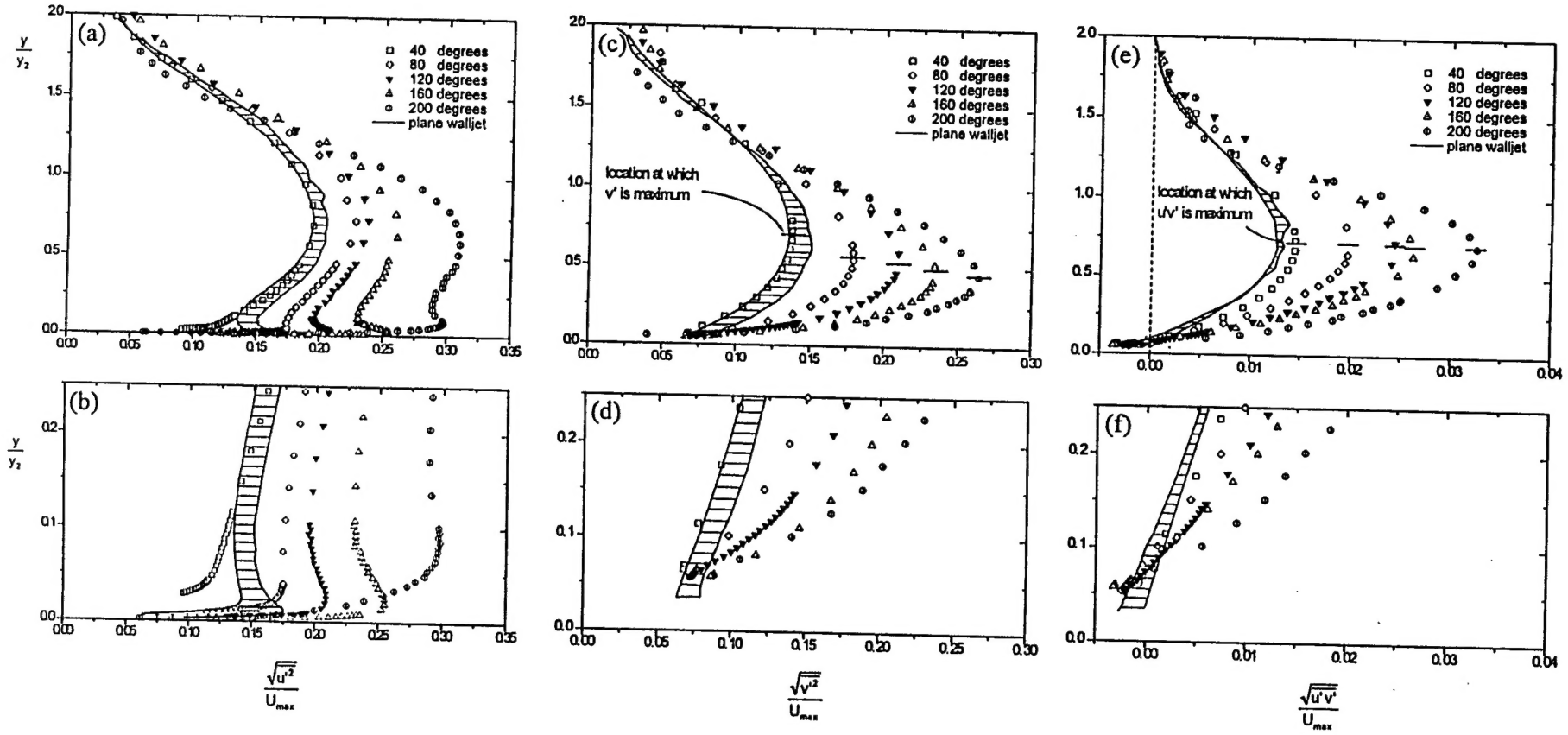
(a)
(b)
(c)
(d)
(e)
(f)
40 degrees
80 degrees
120 degrees
160 degrees
200 degrees
plane walljet
location at which
v' is maximum
location at which
u'v' is maximum
y/y2
√u'2/Umax
√v'2/Umax
√u'v'/Umax

figure 17

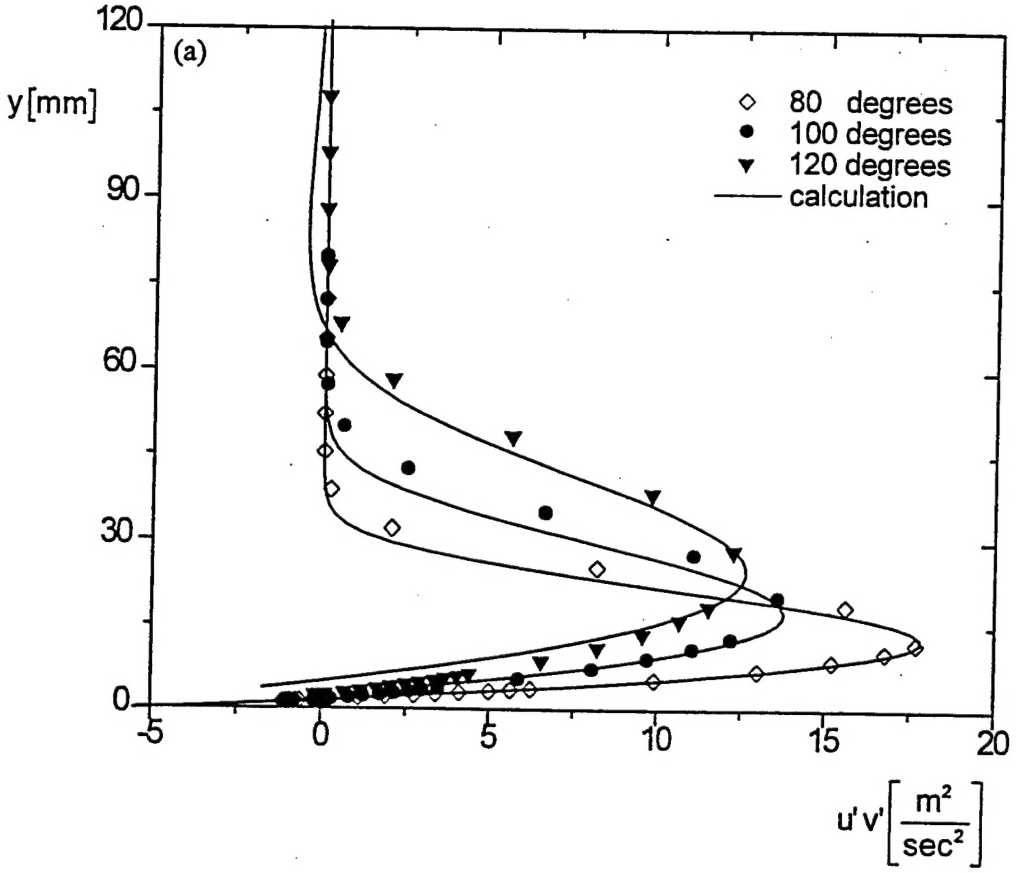
(a)
y[mm]
120
90
60
30
0
-5
0
5
10
15
20
80 degrees
100 degrees
120 degrees
calculation
u'v' [m²/sec²]

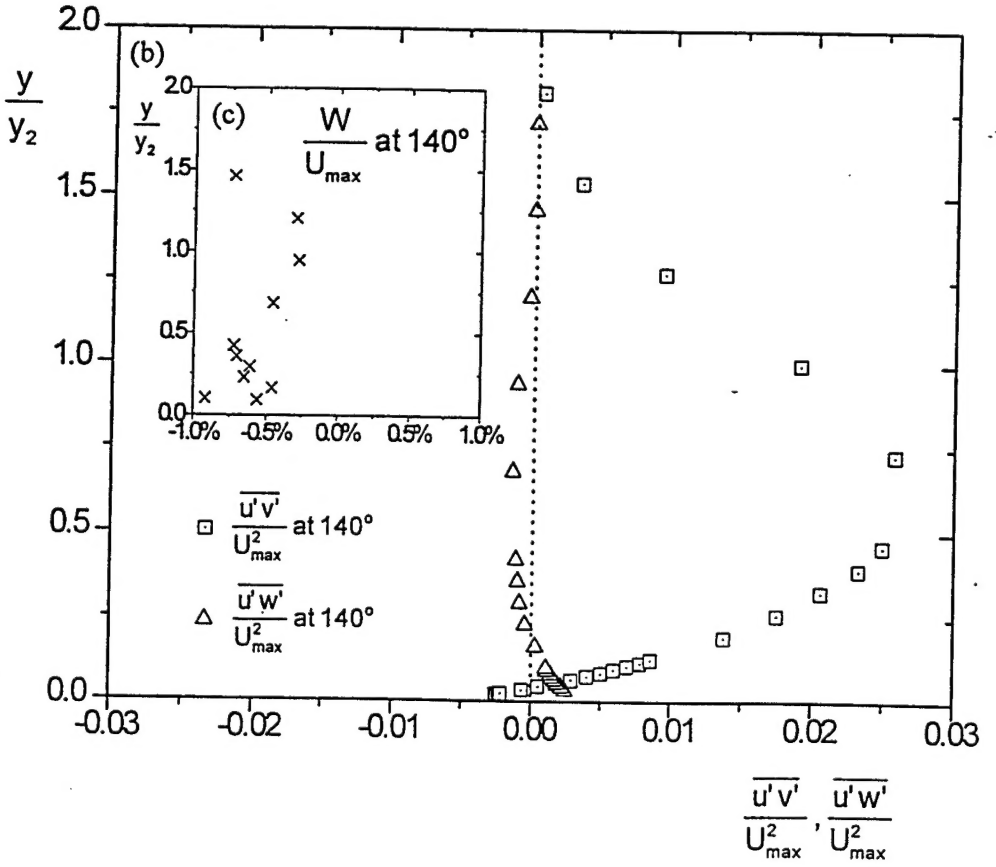
(b)
y/y₂
2.0
1.5
1.0
0.5
0.0
-0.03
-0.02
-0.01
0.00
0.01
0.02
0.03
(c)
W/U_max at 140°
y/y₂
2.0
1.5
1.0
0.5
0.0
-1.0%
-0.5%
0.0%
0.5%
1.0%
u'v'/U²_max at 140°
u'w'/U²_max at 140°
u'v'/U²_max , u'w'/U²_max

figure 19